Measurement of the Turbulence Interaction Noise Generated by Flat Plates with Perforated Leading Edges

Thomas F. Geyer*,

Brandenburg University of Technology Cottbus - Senftenberg, 03046 Cottbus, Germany

The aerodynamic noise generated by the interaction of a turbulent flow with the leading edge of an airfoil is a major source of noise in many applications, such as rotor-stator configurations in turbomachinery. One possible method to reduce this noise is to make the leading edge porous, and hence permeable to the flow, which has been shown to lead to a notable noise reduction in a lot of studies lately. In order to simplify the porous structure and thus to enable a better understanding of the underlying mechanisms, the present study extends this approach to flat plate models modified with a very basic perforation, consisting of evenly spaced circular pores, at their leading edge.

Measurements were performed in an aeroacoustic wind tunnel using microphone array technique and a wind tunnel balance. The results show that perforated leading edges can lead to a notable noise reduction at low frequencies, while the noise at high frequencies is increased, which is assumed to be due to a contribution of surface roughness noise. In the present case, the perforation with the largest pore diameters even lead to a noise increase over the whole range of frequencies at zero angle of attack. Overall, the best performance regarding the noise reduction and the aerodynamics was obtained for perforations with small, but very dense pores.

I. Introduction

The interaction of a turbulent flow with the leading edge of an airfoil is a major source of aerodynamic noise. This so-called turbulence-interaction-noise occurs at the blades of fans and wind turbines as well as at the wings of airplanes. Several methods for the reduction of this noise source mechanism exist, including serrated [1–9] or slitted [10, 11] leading edges or leading edges modified with comb-like structures [12]. Another, very promising approach is the modification of the leading edge with porous or perforated materials [13–20], where noise reductions in the order of 10 dB can be achieved at low and medium frequencies. However, this noise reduction depends on a quite large number of parameters. In addition to the parameters describing the properties of the incoming turbulent flow (such as the flow speed U_0, the turbulence intensity Tu and the integral length scale Λ), this includes the parameters describing the airfoil (the airfoil shape, chord length s and span width b) as well as the parameters used to describe the porous or perforated material. The latter could be macroscopic parameters which presume a homogeneous porous material, such as the air flow resistivity r, the porosity σ and the tortuosity τ, or microscopic parameters that basically describe the shape and size of the pores. However, the description of the porous consistency can still be very complex, especially if the pores are not straight, but twisted, or if the material also contains closed pores that are acoustically ineffective.

*Senior Researcher, Technical Acoustics Group, Brandenburg University of Technology Cottbus - Senftenberg, Germany, thomas.geyer@b-tu.de.

Therefore, in the investigation described in the present paper, which is part of an ongoing study, an approach was chosen that is considerably simpler. The aim is to provide a better insight into the mechanisms that are responsible for the noise reduction, which is done by

1. using a flat plate instead of an airfoil, thus avoiding the additional influence of the airfoil shape and by

2. using a very basic perforation, consisting of evenly spaced, straight circular pores, which can be described easily and enables the calculation of macroscopic parameters like air flow resistivity, porosity and tortuosity.

The remainder of the paper is organized as follows: First, the experimental setup is explained in detail, including the perforated flat plates, the aeroacoustic wind tunnel with the turbulence generators, the microphone array technique and processing of the acoustic data and the wind tunnel balance. Secondly, acoustic and aerodynamic results are presented and finally, a short summary and an outlook are given.

II. Measurement Setup

II.A. Perforated Flat Plates

Measurements were performed on five flat plates with a perforated region at the leading edge. All plates have a chord length of $s = 200$ mm, a span width of $b = 400$ mm and a thickness of $t = 5$ mm. The central part of the span is perforated at the leading edge (with a streamwise extent of 20 mm and a spanwise extent of 250 mm). The perforations consist of evenly spaced circular pores, which were drilled into the plates. A flat plate of the same dimensions, but without perforations was used as a reference. Table 1 lists the different plates, while Figure 1 shows a schematic of one of the perforated plates.

Table 1. Overview of flat plates used for the experiments

Denotation	Pore diameter (mm)	Pore distance (mm)	Porosity (%)
ref	-	-	0
d3_a4	3	4	44.2
d2_a4	2	4	19.6
d1_a4	1	4	4.9
d1_a3	1	3	8.7
d1_a2	1	2	19.6

II.B. Wind Tunnel and Turbulence Generation

All measurements were conducted in the small aeroacoustic open jet wind tunnel [21] at the Brandenburg University of Technology in Cottbus, with a setup similar to that used in [22]. The circular nozzle used has an exit diameter of 0.2 m, leading to a maximum flow speed in the order of 90 m/s, with a low turbulence intensity (below 0.1 % at a flow speed of 50 m/s) and low jet noise. In order to generate the inflow turbulence necessary for the investigation of leading edge noise, different turbulence grids can be attached to the nozzle. In this study, three different grids were used, which are specified in Table 2 (the denotation is chosen in accordance to that used by Roach [23]). They were selected with the aim to obtain a notable range of turbulence intensities and integral length scales, which are known to depend primarily on the bar width or rod diameter of a grid [23]. However, the grids labeled "PPS 15/5" (for "perforated plate with square holes") and "SMR 12.7/0.8" (for "square mesh grid with round rods") were only used for a subset of the measurements. Most measurements were performed with the PPS 11/3 grid.

In order to characterize the inflow turbulence generated by the grids, constant temperature measurements were performed at a distance of 0.2 m from the grid, without the flat plates in place. Those measurements

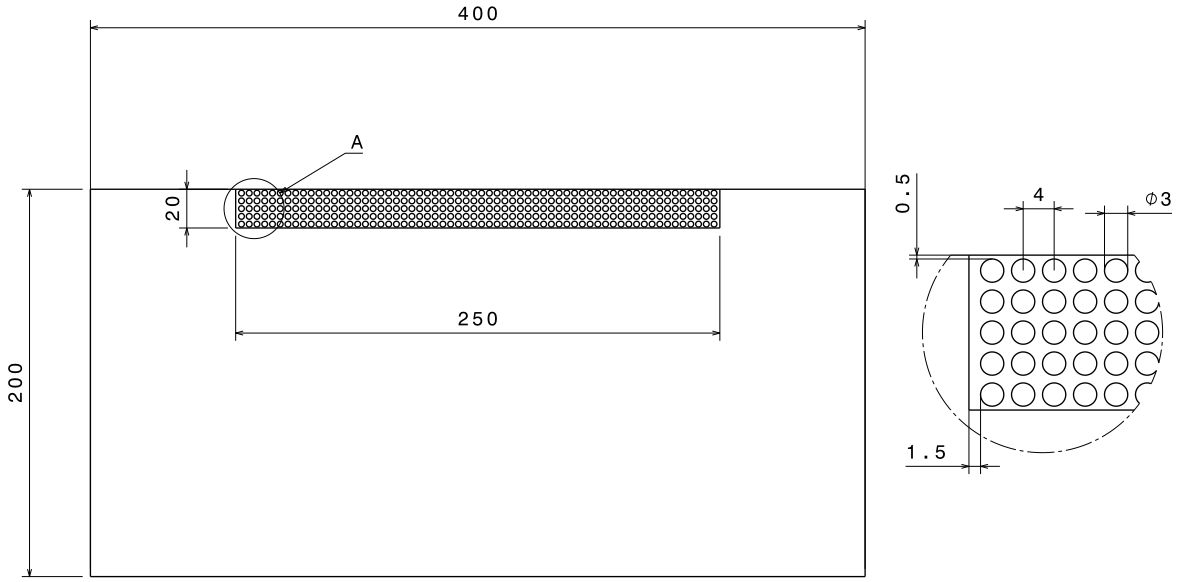

Figure 1. Schematic of the perforated flat plate d3_a4 (all dimensions in mm)

Table 2. Overview of grids used for the generation of the inflow turbulence (notation according to [23])

Denotation	Description	Mesh width (mm)	Bar width/rod diameter (mm)
PPS 11/3	perforated plate with square holes	11	3
PPS 15/5	perforated plate with square holes	15	5
SMR 12.7/0.8	square-mesh array of round rods or wires	12.7	0.8

were done at 31 randomly distributed positions in an area normal to the flow and inside the wind tunnel core jet, using a Dantec single wire probe type P11. Figure 2 shows the turbulence intensity Tu and the streamwise integral length scale Λ_x obtained with the three grids as a function of the flow speed. It is visible that the third grid (SMR 12.7/0.8) leads to strong variations of the integral length scale, but the reasons for those are not clear yet. In this study, acoustic measurements were only performed at two flow velocities, a low flow speed around 20 m/s and a higher flow speed around 40 m/s. Table 3 summarizes the parameters of the flow at both operating points for all three grids.

II.C. Acoustic Measurements and Data Processing

For the acoustic measurements, the plate was positioned at a distance of approximately 0.16 m downstream of the turbulence grids. Please note that this distance is slightly smaller than the distance at which the parameters of the turbulent inflow were measured. Nevertheless, it can be assumed that the turbulence parameters at the position of the leading edge will not be much different from the ones presented in Figure 2. The tips of the plate were attached to a wind tunnel balance to simultaneously measure the aerodynamic performance. Since the span of the plates exceeds the nozzle diameter, no aerodynamic noise was generated at the tips or the lateral mountings. The wind tunnel test section is lined with absorbing foam on the sides and the bottom, leading to a virtually anechoic environment. A schematic of the setup is shown in Figure 3

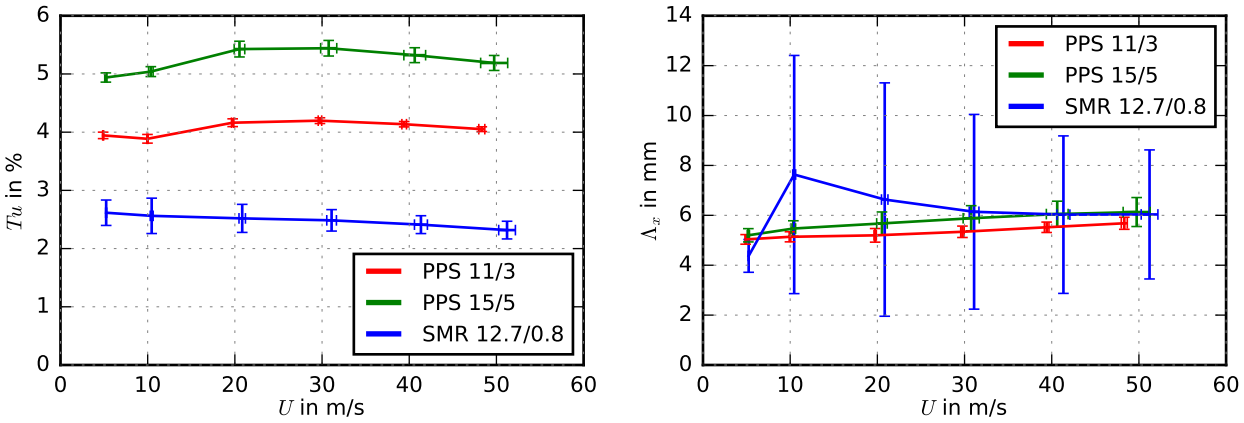

(a) Turbulence intensity

(b) Streamwise integral length scale

Figure 2. Parameters of the turbulent inflow at a distance of 0.2 m from the nozzle

Table 3. Turbulence parameters at the two operating points, "low" and "high" (given are the mean values)

Grid	U **(m/s)**		Tu **(%)**		Λ_x **(mm)**	
	(low)	(high)	(low)	(high)	(low)	(high)
PPS 11/3	19.7	39.4	4.2	4.1	5.2	5.5
PPS 15/5	20.5	40.6	5.4	5.3	5.7	6.1
SMR 12.7/0.8	20.8	41.3	2.5	2.4	6.6	6.0

and a photograph in Figure 4. The acoustic measurements were performed using a planar microphone array, which was positioned out of the flow, at a distance of 0.71 m above the plates. It consists of 56 1/4th inch microphone capsules flush mounted into an aluminum plate with dimensions of 1.5 m × 1.5 m. The acoustic data were recorded with a sampling frequency of 51.2 kHz and a duration of 40 s using a National Instruments 24 Bit multichannel measurement system. In post-processing, the data were transferred to the frequency domain using a Fast Fourier Transformation according to Welchs method [24], with blocks of 4,096 samples and an overlap of 50 % obtained by the Hanning window function. The resulting cross-spectral matrices were further processed using the CLEAN-SC beamforming algorithm [25] integrated in the *Acoular* open source software package [26,27], which was applied to a two-dimensional focus grid parallel to the microphone array and aligned with the flat plate leading edge. The focus grid had dimensions of 0.6 m × 0.6 m with a resolution of 5 mm. A fast ray tracing method [28] was employed to correct for the effect of the wind tunnel shear layer on the noise source localization.

In order to quantify noise generated at the leading edge of the plates due to the interaction with incident turbulence, only those noise contributions located within a region around the leading edge were integrated. This leading edge sector, which is included in the schematic shown in Figure 3, has a spanwise extent of 0.1 m and a streamwise extent of 0.13 m. It is located entirely inside the wind tunnel core jet and thus only contains the noise source of interest, but no unwanted noise sources such as the trailing edge of the plate or the turbulence grid. Finally, the resulting sound pressure was converted to sound pressure levels L_p *re* 20 μPa and 6 dB were subtracted to account for the reflection at the rigid microphone array plate.

In addition to the sound pressure level spectra, maps of the noise source locations were derived from the beamforming results (so-called sound maps). This was not done with the CLEAN-SC algorithm, but with the functional beamforming [29] due to the fact that the latter can produce continuous source distributions with high dynamic range.

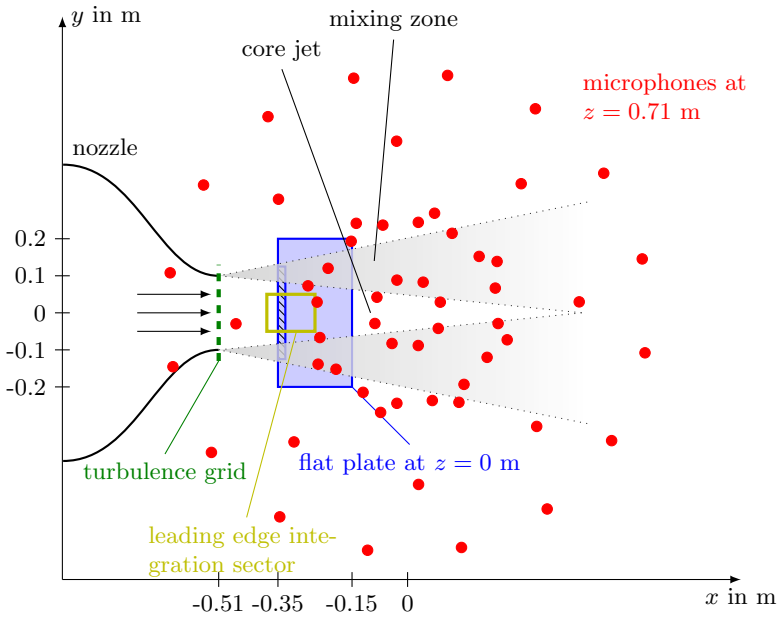

Figure 3. Schematic display of the measurement setup (top view), the hatched area symbolizes the perforated part of the flat plate

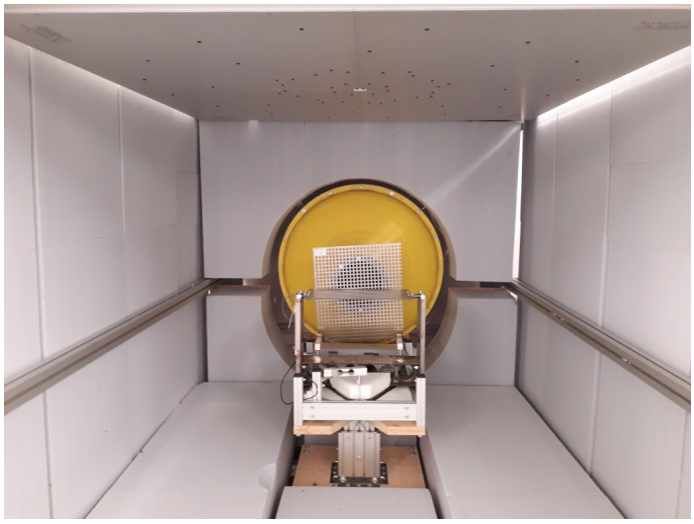

Figure 4. Photograph of the setup in the aeroacoustic wind tunnel

II.D. Aerodynamic Measurements

Simultaneous to the acoustic measurements, the aerodynamic performance was captured by measuring the time-averaged lift force F_L and drag force F_D acting on the perforated plates using a wind tunnel balance. The results were analyzed using an in-house software. Measurements were performed at two geometric angles of attack of 0° and 15°. It has to be noted that with the present setup, consisting of flat plate models immersed into a cone-shaped open jet without side plates (see Figure 3), standard correction procedures that transfer the geometric angle of attack into an effective one that would be measured in free air (like the well-known method proposed by Brooks et al. [30]) cannot be used. Instead, geometrical angles of attack will be given throughout the paper.

III. Results

III.A. Acoustic Results

In a first comparison, functional beamforming sound maps are shown in Figure 5 for all flat plates of the current study, subjected to the inflow turbulence generated by the PPS 11/3 turbulence grid at zero angle of attack and the higher flow velocity of 40 m/s. Some general trends are immediately visible: Regarding the overall noise source contributions it can be observed that at low frequencies the main noise source is the leading edge of the flat plates, which is especially visible for the one third octave bands with center frequencies of 500 Hz and 1 kHz. With increasing frequency, the noise source at the turbulence grid becomes more and more visible until it is clearly the dominant noise source at the one third octave band with the highest center frequency of 8 kHz. Regarding the effect of the perforations, it can be seen that some of the perforations do not lead to a noise reduction at all, but rather increase the noise, while others are very efficient in reducing the noise. The first is especially true for the d3_a4 perforated plate, which is the one having pores with the largest diameter of 3 mm. It is possible that for this plate, noise is generated by the flow over the perforations, which constitute a very rough surface. Since the angle of attack was zero in the cases shown in the sound maps, the increased noise cannot be due to small jets coming out of the pores, since that would require a pressure difference between the two sides (suction side and pressure side). Other perforated plates lead to notable noise reductions. For example, at the lowest one third octave band with a center frequency of 500 Hz, the d2_a4 and d1_a2 perforated flat plates perform best. These plates have the same porosity of 19.6 %, which is the second highest value after that of the d3_a4 plate with $\sigma = 44.2$ %. At the remaining one third octave bands it is more complicated to judge the performance of the perforated plates compared to the baseline, since the maximum of the dynamic range is determined by the d3_a4 perforated plate, which clearly generates the highest noise levels.

Thus, in a second step, one third octave band sound pressure level spectra are analyzed as a more quantitative means to investigate the effect of different perforations. As described in Section II.C, they were obtained by integrating all contributions from noise sources located within the chosen leading edge sector, and hence the noise generated by the turbulence grid is not included.

Figure 6 shows one third octave band sound pressure level spectra obtained with the PPS 11/3 turbulence grid at 0° angle of attack, while Figure 7 shows the results at a geometric angle of attack of 15°. For the zero angle of attack case, it is again visible that the perforated plate with the largest holes (d3_a4) does not lead to a noise reduction at all, while the other perforated plates at least result in a noise reduction at low to medium frequencies. At the one third octave band with a center frequency of 800 Hz at the lower flow speed (Figure 6(a)), a very high noise reduction can be seen especially for the perforated flat plates d2_a4, d1_a3 and d1_a2, which is in the order of 10 to 15 dB. It is presently not clear whether this is a physically meaningful result or only a consequence of the CLEAN-SC beamforming algorithm failing to locate all the corresponding noise sources in the integration sector. Future tests involving different beamforming algorithms, such as DAMAS [31] or orthogonal beamforming [32], are planned to further analyze this effect. Apart from this single case, noise reductions in the lower frequency range are in the order of approximately 3 dB to 5 dB. The perforated flat plates that give the highest noise reduction are the d1_a3 and d1_a2 plates, and hence those with the smallest pore diameters and the smallest pore distances. At one third octave bands with center frequencies of 400 Hz and 500 Hz, two of the perforated flat plates (d2_a4 and d1_a2) also generate slightly more noise than the reference flat plate. The reason for this increase is not clear yet. At high frequencies, the noise generated by the perforated plates notably exceeds the noise by the reference plate, which is assumed to be due to a contribution of roughness noise caused by the flow over the perforations. This hypothesis is supported by the fact that the perforations with the largest pores generate the highest noise in this frequency range. In addition, for the plates with pores of 1 mm diameter the plates with the highest porosity generate more high frequency noise than the plates with a lower porosity. Regarding the two perforated plates with different pore sizes, but identical porosities (d2_a4 and d1_a2) the observed trend leads to the fact that the noise generated by the perforated plate with the larger pores (d2_a4) exceeds the noise of the reference flat plate already at a frequency of 1.6 kHz at the low flow speed and 2 kHz at the higher flow speed, while this frequency is much higher for the perforated plate with the smaller pores (d1_a2),

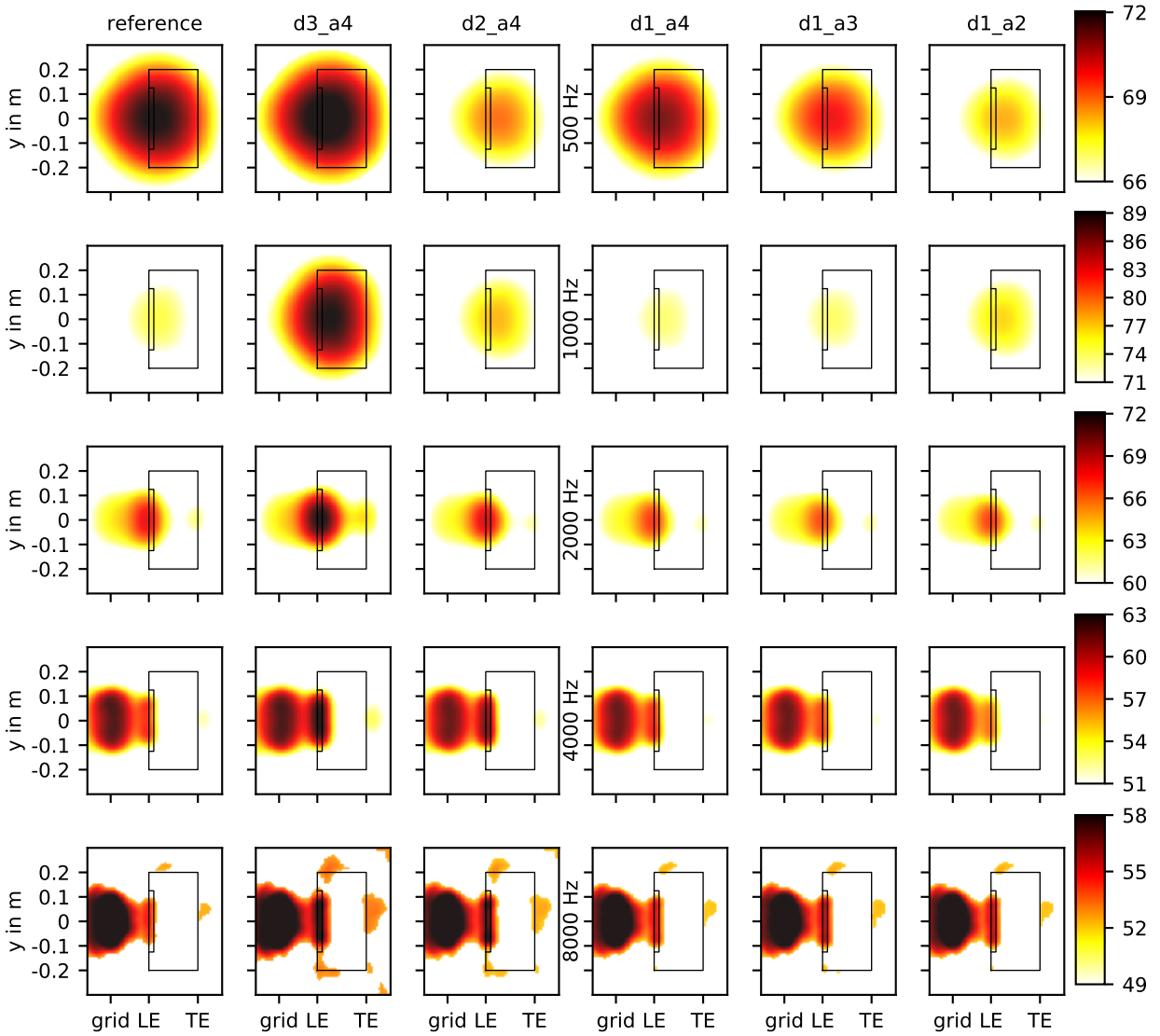

Figure 5. One third octave band sound maps obtained for the flat plate models from Table 1 at a flow speed of 40 m/s and an angle of attack of 0°; inflow turbulence generated by the PPS 11/3 turbulence grids; flow from left to right; location of the turbulence grid ("grid"), the leading edge ("LE") and the trailing edge ("TE") of the flat plate are indicated (please note the different dynamic ranges for the different one third octave bands)

with values of 2.5 kHz and 5 kHz, respectively.

When the angle of attack is increased to 15°, all perforated plates lead to a noise reduction at low and medium frequencies (up to 1.25 kHz for the lower flow speed of 20 m/s, Figure 7(a), and up to 2.5 kHz for the higher flow speed, Figure 7(b)), even the perforated plate with the largest pore diameters (d3_a4), while the noise increase at high frequencies is still visible. The fact that the frequency region, at which the perforations lead to a noise reduction, increases with flow speed is very interesting, as it indicates that an even better overall noise reduction may be observed for applications that work at very high Reynolds numbers. Overall, the highest noise reductions at low frequencies at this angle of attack are visible for the d2_a4 and the d1_a2 perforated flat plates, which are the ones that have the same high porosity of 19.6 %, but again the one with the larger pores (d2_a4) will lead to a noise increase compared to the reference flat plate at considerably lower frequencies than the one with the smaller pores (d1_a2).

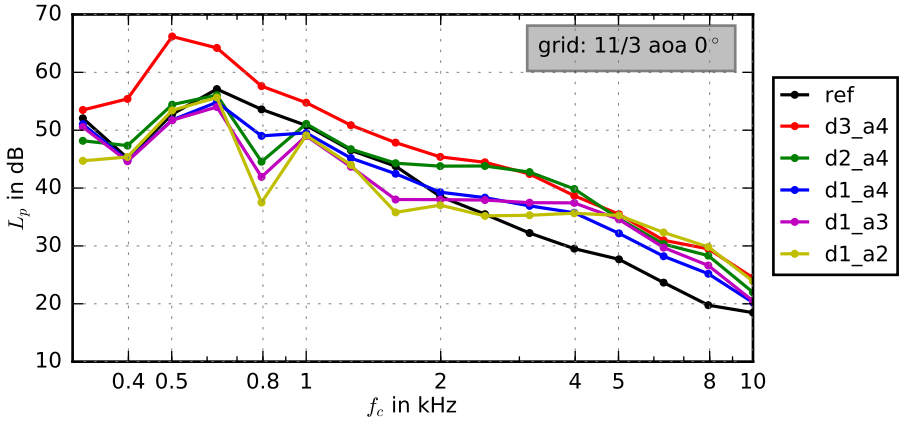

(a) Low flow speed ($U \approx 20$ m/s)

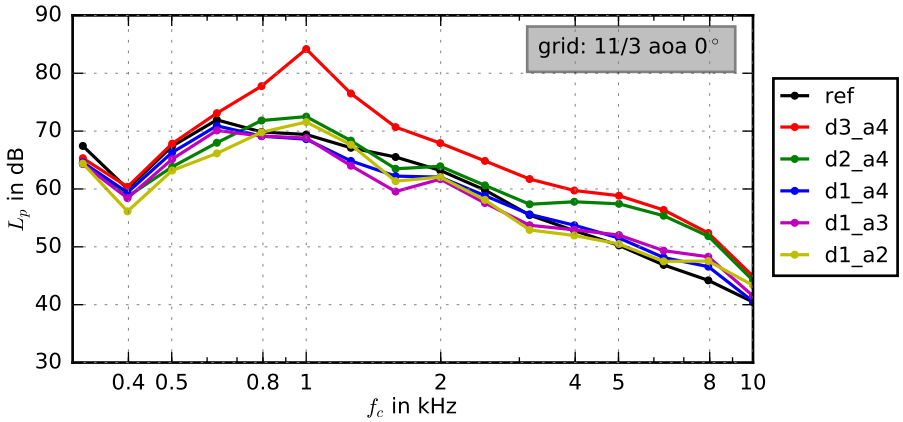

(b) High flow speed ($U \approx 40$ m/s)

Figure 6. Resulting sound pressure level spectra generated by the flat plates at 0° geometric angle of attack at two velocities (PPS 11/3 turbulence grid)

In a next step it was investigated how the parameters of the inflow turbulence affect the resulting sound pressure level spectra. This was done using all three turbulence grids specified in Table 2, but only for the reference flat plate and the perforated plate with the largest pores (d3_a4). Since it has been shown that this particular perforated plate does not lead to a noise reduction at zero angle of attack, these comparisons are only made for the higher geometric angle of attack of 15°. The results are shown in Figure 8, again for the two flow speeds of 20 m/s and 40 m/s. The turbulence generated by the different grids shows strong differences regarding the intensity, but comparable results regarding the integral length scale (see Figure 2). Thus, as expected, the spectra differ mainly regarding their amplitude, while the spectral shapes remain similar. The highest levels were measured for the flat plates in the turbulence generated by the PPS 15/5 grid, which gives the highest turbulence intensity of about 5.3 %. The lowest levels were obtained with the SMR 12.7/0.8 grid, which generates the turbulence with the lowest intensity of about 2.5 %. Interestingly, the differences are much more distinct for the unperforated baseline flat plate than for the perforated flat plate, especially at high frequencies. It is reasonable to assume that the ratio of the size of the turbulent eddies, and hence the integral length scale of the incoming turbulence, to the pore diameter will affect the potential noise reduction. However, since the integral length scale is similar for the turbulence grids used in the present study (see Figure 2(b)), this influence cannot be examined here.

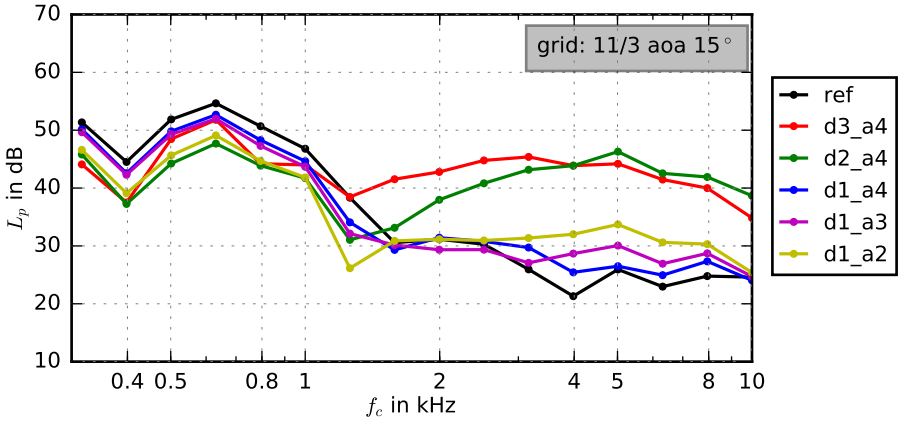

(a) Low flow speed ($U \approx 20$ m/s)

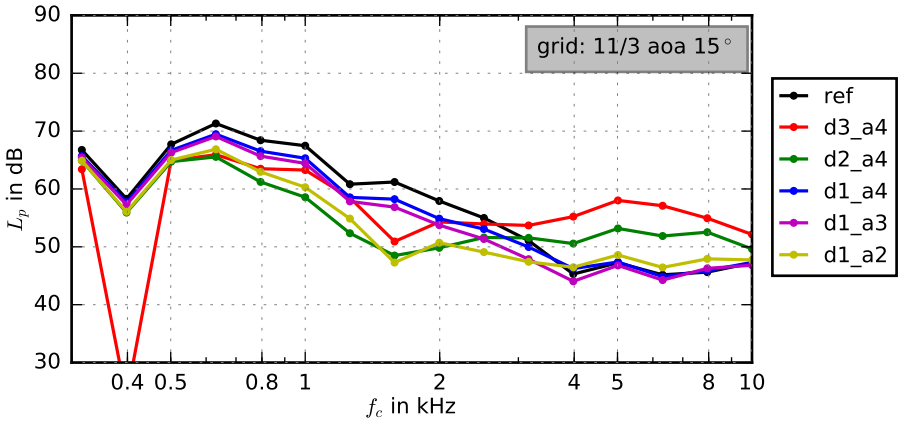

(b) High flow speed ($U \approx 40$ m/s)

Figure 7. Resulting sound pressure level spectra generated by the flat plates at 15° geometric angle of attack at two velocities (PPS 11/3 turbulence grid)

III.B. Aerodynamic Results

Since at zero angle of attack the flat plates generate no lift force, the influence of the perforations on the aerodynamic performance will only be shown for the measurements at a geometric angle of attack of 15°. Figure 9 shows normalized forces at the lower flow speed of about 20 m/s and Figure 10 those at 40 m/s. As expected, the perforated plate with the highest porosity (d3_a4 with $\sigma = 44.2$ %) gives the lowest lift (87 % and 86 % of that obtained for the reference flat plate at 20 m/s and 40 m/s, respectively) and the highest drag (111 % and 112 % of that obtained for the reference flat plate). The perforated plates with the lowest porosities (d1_a4 with $\sigma = 4.9$ % and d1_a3 with $\sigma = 8.7$ %) generate the highest lift, with values between 98 % and 99 % of those obtained for the reference flat plate, and the lowest drag, with values that are between 1 % to 6 % increased compared to the baseline. Overall, the best aerodynamic performance can be observed for the perforated flat plate with the smallest porosity (d1_a4). Interestingly, when the results of the two plates with identical porosities ($\sigma = 19.6$ %), but different pore sizes ($d = 2$ mm for the d2_a4 perforated plate and $d = 1$ mm for the d1_a2 perforated plate) are compared, it can be seen that the plate with the larger pores (d2_a4) has a slightly higher drag force, with values of 111 % and 112 % of the drag measured for the reference flat plate at 20 m/s and 40 m/s, respectively, compared to the plate with the smaller pores (108 % and 110 %). Considering the accuracy of the aerodynamic measurements, especially regarding the adjustment of the angle of attack, the lift forces are the same for both perforated plates. Thus, from an aerodynamic standpoint, it is advantageous to use denser perforations with smaller pores sizes than

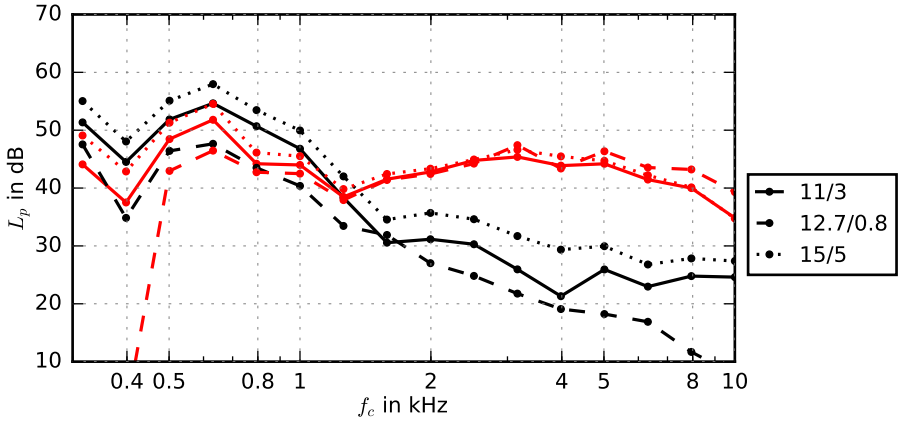

(a) Low flow speed ($U \approx 20$ m/s)

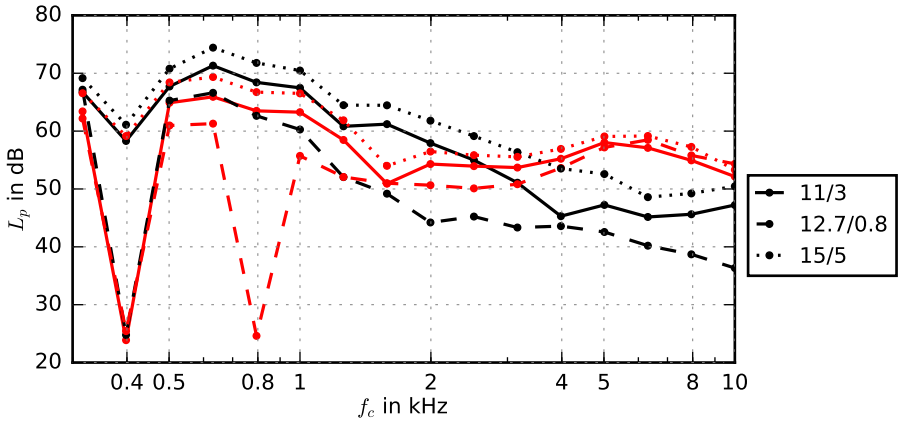

(b) High flow speed ($U \approx 40$ m/s)

Figure 8. Resulting sound pressure level spectra generated by two of the plates (black: reference, red: d3_a4) at velocities of 20 m/s and 40 m/s and a geometric angle of attack of 15° using different turbulence grids

sparser perforations with larger pores, even if the resulting porosity is the same, since larger pores result in an increase in drag.

IV. Summary and Outlook

As part of an ongoing experimental study on the reduction of airfoil turbulence interaction noise, the noise generation and the aerodynamic performance of flat plates modified with regular perforations in a region close to the leading edge were investigated. Thereby, the idea is to fundamentally simplify the setup by using straight pores (instead of the more complex pore structures that can be found in typical porous absorbers such as metal foams, polyurethane foams or felts) and flat plates instead of airfoils (and hence eliminating the additional influence of the airfoil shape), thus enabling a better understanding of the basic trends and physical mechanisms. The perforations consist of evenly spaced circular holes and are characterized by the pore diameter and the pore distance. Measurements on the flat plate models were performed in an aeroacoustic open jet wind tunnel, using a planar 56-channel microphone array and a wind tunnel balance. The inflow turbulence required for the investigation of turbulence interaction noise was provided by three different turbulence grids, which were attached to the nozzle exit. Two geometric angles of attack (0° and 15°) and two different flow speeds (20 m/s and 40 m/s) were adjusted.

In general, the perforated plates were found to lead to a noise reduction at low and medium frequencies

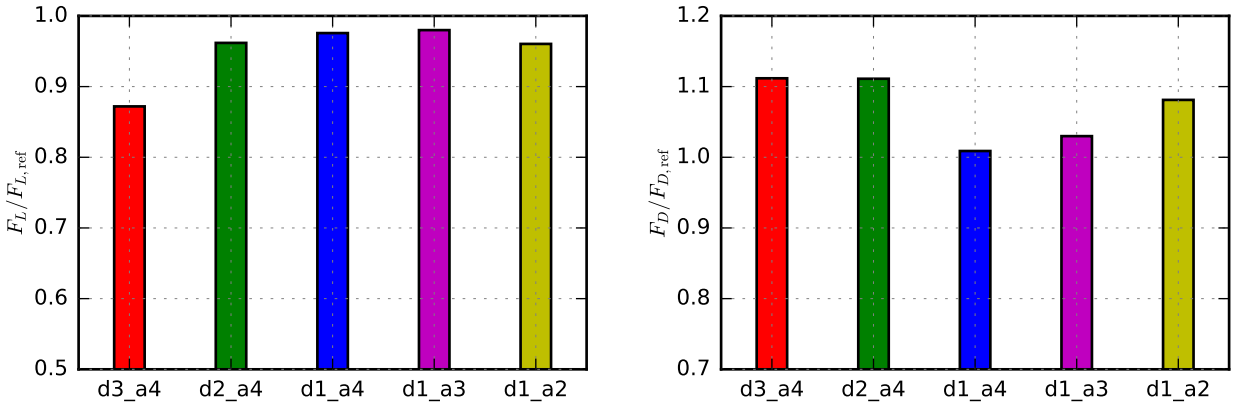

(a) Lift force

(b) Drag force

Figure 9. Aerodynamic forces of the perforated plates (normalized with the force of the reference plate) at a flow speed of approximately 20 m/s and a geometric angle of attack of 15° (PPS 11/3 turbulence grid)

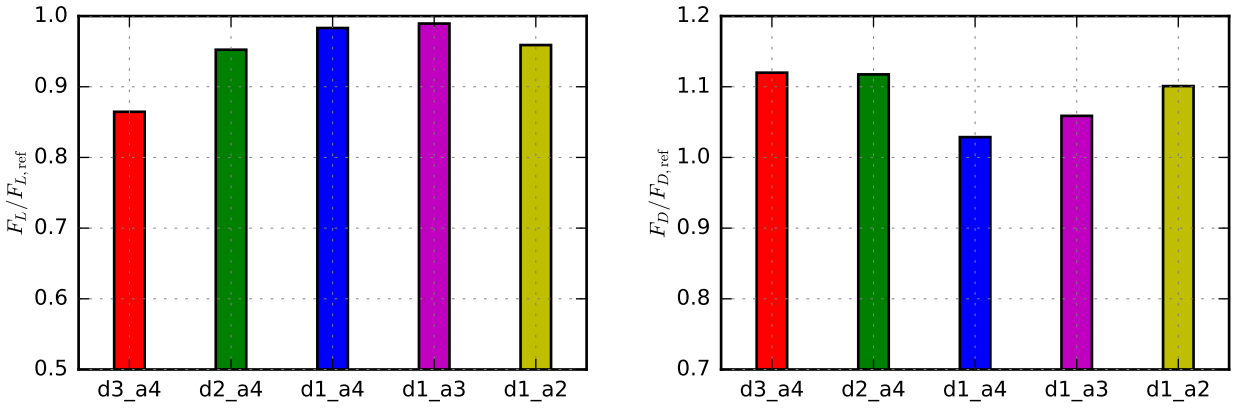

(a) Lift force

(b) Drag force

Figure 10. Aerodynamic forces of the perforated plates (normalized with the force of the reference plate) at a flow speed of approximately 40 m/s and a geometric angle of attack of 15° (PPS 11/3 turbulence grid)

compared to an unperforated reference plate. The only exception was the flat plate with the largest pores with a diameter of 3 mm at zero angle of attack, which generated more noise than the reference flat plate over the hole range of frequencies. The reason for this noise increase is not fully clear yet, but it can be assumed that a contribution of surface roughness noise is at least partially responsible. At high frequencies, all perforations lead to a noise increase, which is clearly due to surface roughness noise. Overall, it was found that small pores with a high pore density (and hence a relatively high porosity) are most efficient both regarding a low noise generation and a high aerodynamic performance. Future tests are planned on additional flat plates modified with even smaller pores and smaller pore distances to see if this trend continues.

References

[1]Hersh, A. S., Soderman, P. T., Hayden, R. E., Investigation of acoustic effects of leading-edge serrations on airfoils. Journal of Aircraft, 11(4), 197-202, 1974.

[2]Hansen, K. L., Kelso, R. M., Dally, B. B., Performance variations of leading-edge tubercles for distinct airfoil profiles. AIAA journal, 49(1), 185-194, 2011.

[3]Clair, V., Polacsek, C., Le Garrec, T., Reboul, G., Gruber, M., Joseph, P., Experimental and numerical investigation of turbulence-airfoil noise reduction using wavy edges. AIAA journal, 51(11), 2695-2713, 2013.

[4]Narayanan, S., Chaitanya, P., Haeri, S., Joseph, P., Kim, J. W., Polacsek, C., Airfoil noise reductions through leading edge serrations. Physics of Fluids, 27(2), 2015.

[5]Biedermann, T. M., Chong, T. P., Kameier, F., Paschereit, C. O., Statistical–empirical modeling of airfoil noise subjected to leading-edge serrations. AIAA Journal, 3128-3142, 2017.

[6]Chaitanya, P., Joseph, P., Narayanan, S., Vanderwel, C., Turner, J., Kim, J. W., Ganapathisubramani, B., Performance and mechanism of sinusoidal leading edge serrations for the reduction of turbulence–aerofoil interaction noise. Journal of Fluid Mechanics, 818, 435-464, 2017.

[7]Chaitanya, P., Joseph, P., Narayanan, S., Kim, J. W., Aerofoil broadband noise reductions through double-wavelength leading-edge serrations: a new control concept. Journal of Fluid Mechanics, 855, 131-151, 2018.

[8]Juknevicius, A., Chong, T. P., On the leading edge noise and aerodynamics of thin aerofoil subjected to the straight and curved serrations. Journal of Sound and Vibration, 425, 324-343, 2018.

[9]Biedermann, T. M., Czeckay, P., Geyer, T. F., Kameier, F., Paschereit, C. O., Effect of inflow conditions on the noise reduction through leading edge serrations. AIAA Journal, 1-6, 2019.

[10]Chaitanya, P., Joseph, P., Slitted leading edge profiles for the reduction of turbulence-aerofoil interaction noise. The Journal of the Acoustical Society of America, 143(6), 3494-3504, 2018.

[11]Chaitanya, P., Joseph, P., Ayton, L. J., Leading-edge profiles for the reduction of airfoil interaction noise. AIAA Journal, 1-12, 2019.

[12]Geyer, T. F., Wasala, S. H., Sarradj, E., Experimental study of airfoil leading edge combs for turbulence interaction noise reduction. Acoustics, Vol. 2, No. 2, pp. 207-223, Multidisciplinary Digital Publishing Institute, 2020.

[13]Lee, S., Reduction of blade-vortex interaction noise through porous leading edge. AIAA Journal, 32(3), 480-488, 1994.

[14]Tinetti, A., Kelly, J., Thomas, R., Bauer, S., Reduction of wake-stator interaction noise using passive porosity. In: Proceedings of the 40th AIAA Aerospace Sciences Meeting and Exhibit, AIAA paper 2002-1036, 2002.

[15]Geyer, T. F., Sarradj, E., Giesler, J., Hobracht, M., Experimental assessment of the noise generated at the leading edge of porous airfoils using microphone array techniques. In: Proceedings of the 17th AIAA/CEAS Aeroacoustics Conference, AIAA paper 2011-2713, 2011.

[16]Roger, M., Schram, C., De Santana, L., Reduction of airfoil turbulence-impingement noise by means of leading-edge serrations and/or porous materials. In: Proceedings of the 19th AIAA/CEAS Aeroacoustics Conference, AIAA paper 2013-2108, 2013.

[17]Geyer, T. F., Lucius, A., Schrödter, M., Schneider, M., Sarradj, E., Reduction of turbulence interaction noise through airfoils with perforated leading edges. Acta Acustica united with Acustica, Vol. 105 (1), 109 - 122, 2019.

[18]Sinnige, T., Corte, B. D., De Vries, R., Avallone, F., Merino-Martínez, R., Ragni, D., Eitelberg, G., Veldhuis, L. L., Alleviation of propeller-slipstream-induced unsteady pylon loading by a flow-permeable leading edge. Journal of Aircraft, 56(3), 1214-1230, 2019.

[19]Zamponi, R., Van de Wyer, N., Schram, C. F., Experimental investigation of airfoil turbulence-impingement noise reduction using porous treatment. In: Proceedings of the 25th AIAA/CEAS Aeroacoustics Conference, AIAA paper 2019-2649, 2019.

[20]Ocker, C., Pannert, W., Merkel, M., Geyer, T. F., Czwielong, F., Becker, S., Krömer, F., Experimental Investigation of the impact of 3D-metal-printed perforated leading edges on airfoil and axial fan noise. In: Proceedings of the 26th AIAA/CEAS Aeroacoustics Conference, AIAA paper 2020-2529, 2020.

[21]Sarradj, E., Fritzsche, C., Geyer, T. F., Giesler, J., Acoustic and aerodynamic design and characterization of a small-scale aeroacoustic wind tunnel, Applied Acoustics, 70, 1073-1080, 2009.

[22]Geyer, T. F., Sarradj, E., Giesler, J., Application of a beamforming technique to the measurement of airfoil leading edge noise. Adv Acoust Vib, Vol. 2012, 2012.

[23]Roach, P. W., The generation of nearly isotropic turbulence by means of grids. Int J Heat Fluid Flow, 8(2), 82-92, 1987.

[24]Welch, P. D., The use of fast Fourier transform for the estimation of power spectra: a method based on time averaging over short, modified periodograms. IEEE Trans. Audio and Electroacoustics, 15(2), 70–73, 1967.

[25]Sijtsma, P., CLEAN based on spatial source coherence. International Journal of Aeroacoustics, 6(4), 357-374, 2007.

[26]Sarradj, E., Herold, G., A Python framework for microphone array data processing. Applied Acoustics, 116, 50-58, 2017.

[27]Herold, G., Sarradj, E., Open-source software for the application of microphone array methods. Noise & Vibration Worldwide, 48(3-4), 44-51, 2017.

[28]Sarradj, E., A fast ray casting method for sound refraction at shear layers. International Journal of Aeroacoustics, Vol 16, Issue 1-2, 65–77, 2016.

[29]Dougherty, R. P., Functional beamforming for aeroacoustic source distributions. In: Proceedings of the 20th AIAA/CEAS Aeroacoustics Conference, AIAA paper 2014-3066, 2014.

[30]Brooks, T. F., Marcolini, M. A., Pope, D. S., Airfoil trailing edge flow measurements and comparison with theory, incorporating open wind tunnel corrections. In: Proceedings of the 9th Aeroacoustics Conference, AIAA paper 84-2266, 1984.

[31]Brooks, T. F., Humphreys, W. M., A deconvolution approach for the mapping of acoustic sources (DAMAS) determined from phased microphone arrays. Journal of Sound and Vibration, 294(4-5), 856-879, 2006.

[32]Sarradj, E.,. A fast signal subspace approach for the determination of absolute levels from phased microphone array measurements. Journal of Sound and Vibration, 329(9), 1553-1569, 2010.